

MedChemComm

Accepted Manuscript



This is an *Accepted Manuscript*, which has been through the Royal Society of Chemistry peer review process and has been accepted for publication.

Accepted Manuscripts are published online shortly after acceptance, before technical editing, formatting and proof reading. Using this free service, authors can make their results available to the community, in citable form, before we publish the edited article. We will replace this *Accepted Manuscript* with the edited and formatted *Advance Article* as soon as it is available.

You can find more information about *Accepted Manuscripts* in the [Information for Authors](#).

Please note that technical editing may introduce minor changes to the text and/or graphics, which may alter content. The journal's standard [Terms & Conditions](#) and the [Ethical guidelines](#) still apply. In no event shall the Royal Society of Chemistry be held responsible for any errors or omissions in this *Accepted Manuscript* or any consequences arising from the use of any information it contains.



Design, synthesis, *in vivo* evaluations of benzyl N^ω-nitro-N^α-(9H-pyrido[3,4-b]indole-3-carbonyl)-L-argininate as apoptosis inducer capable of decreasing serum concentration of P-selectin[†]

Wenyun Xu,^a Ming Zhao,^{a,b,*} Yuji Wang,^a Haimei Zhu,^a Yaonan Wang,^a Shurui Zhao,^a Jianhui Wu,^a and Shiqi Peng^{a,*}

A series of findings suggest that the discovery of *in vivo* apoptosis inducers for chemotherapy is of clinical importance. Based on the analyses of the pharmacophores of *in vitro* apoptosis inducers, the correlation of P-selectin and apoptosis and the docking investigation of benzyl N^ω-nitro-N^α-(9H-pyrido[3,4-b]indole-3-carbonyl)-L-argininate (NRCB) was designed as a novel nano-scale apoptosis inducer capable of decreasing serum concentration of P-selectin *in vivo*. The rationality of the design was confirmed by NRCB effectively promoting the apoptosis of K562 cells *in vitro*, dose-dependently decreasing the concentration of P-selectin in the serum of S180 mice, and concentration dependently forming nanoparticles. FT-MS and NOESY 2D NMR spectra defined NRCB forming a hexamer of triangle-like conformation. At 0.01, 0.1 and 1 μmol/kg of doses NRCB effectively decreased tumor weights and sizes of S180 mice in a dose-dependent manner, and the minimal effective dose was 0.01 μmol/kg. At 1 μmol/kg of dose NRCB also effectively inhibited xylene-induced ear edema and decreased the serum TNF-α and IL-2 of the treated mice. The correlations between apoptosis with P-selectin, TNF-α and IL-2 were discussed in particular. In conclusion, NRCB is a novel nano-scale apoptosis inducer capable of decreasing serum concentration of P-selectin *in vivo*, and could be a promising lead compound of apoptosis inducers for chemotherapy.

Received 00th January 20xx,
Accepted 00th January 20xx

DOI: 10.1039/x0xx00000x

www.rsc.org/

Introduction

Cell death plays a crucial role in cancer and myocardial infarction, occurring through distinct pathways, including apoptosis, necrosis and autophagy.¹ Apoptosis is initially introduced to describe cell death modality, consisting of cell shrinkage, chromatin granule condensation, loss of nuclear membrane integrity, semi-permeable membrane blebbing and eventually apoptotic body formation.² Accumulating evidence suggests that there is a relationship between apoptosis, necrosis and autophagy.³ In normal cell homeostasis and in the development of a variety of human diseases, apoptosis plays a critical role.⁴ Inadequate apoptosis could over-raise the proliferation of cancer cells.⁵ A series of clinical drugs exhibit chemotherapeutic potencies at least partially through inducing apoptosis.^{6–8} The discovery of apoptosis inducers to develop new chemotherapeutic agents has been one of the interests of researchers.^{9–13} Apoptosis

inducers of diverse structures, such as pyrazoline derivatives bearing a phenyl pyridazine core,¹⁴ dehydroabiatic acid thiourea derivatives containing a bisphosphonate moiety,¹⁵ betulin acid ester derivatives,¹⁶ and zinc (II) complex of 5-bromo-8-hydroxyquinoline,¹⁷ are known. β-Carbolines, indole-2-carboxylic acid benzylidenehydrazides and Cl-amidine are another class of interesting apoptosis inducers.^{18–22} These apoptosis inducers were evaluated *in vitro* only, and *in vivo* active apoptosis inducer remains unknown. On the other hand, the side effects of some first-line antitumor drugs including cisplatin and doxorubicin are a result of the induced apoptosis of them.^{23–26} Tumor growth can be significantly slowed in the absence of P-selectin, and recently high tumor cell apoptosis was observed in tumors growing in P-selectin^{-/-} mice.²⁷

In this context, by using the pharmacophores of the β-carbolines, indole-2-carboxylic acid benzylidenehydrazides and Cl-amidine as building blocks, and by using the correlation between apoptosis and P-selectin as a molecular mechanism linker, benzyl N^ω-nitro-N^α-(9H-pyrido[3,4-b]indole-3-carbonyl)-L-argininate (NRCB), a novel apoptosis inducer capable of down-regulating P-selectin, was designed. Fig. 1 indicates that the interactions between NRCB and the amino acid residues of the active pocket of P-selectin are eight hydrogen bonds, including two hydrogen bonds formed by the oxygen of NH=C-NH-NO₂ of NRCB and the H of the NH₂ of the side chain of Lys84 of the active pocket, two hydrogen bonds formed by the H of NH=C-NH-NO₂ of NRCB and the two oxygens of

^a Beijing area major laboratory of peptide and small molecular drugs; Engineering Research Center of Endogenous Prophylactic of Ministry of Education of China; Beijing Laboratory of Biomedical Materials; College of Pharmaceutical Sciences, Capital Medical University, Beijing 100069, P.R. China.

^b Faculty of Biomedical Science and Environmental Biology, Kaohsiung Medical University, Kaohsiung, Taiwan.

* SP: Tel: +86-10-8391-1528, E-mail: sqpeng@bjmu.edu.cn; MZ: Tel: +86-10-8391-1535, E-mail: mingzhao@bjmu.edu.cn.

[†] The authors declare no competing interests.

Electronic supplementary information (ESI) available. See DOI:

carbonyl of Glu88 of the active pocket, a hydrogen bond formed by the H of $\text{NH}=\text{C}-\text{NH}-\text{NO}_2$ of NRCB and the oxygen of carbonyl of Glu88 of the active pocket, a hydrogen bond formed by the H of 3-carbonyl-NH of NRCB and the oxygen of carbonyl of Glu107 of the active pocket, a hydrogen bond formed by the H of the side chain OH of Try94 of the active pocket and the 2-N of NRCB, as well as a hydrogen bond formed by the H of the side chain OH of Ser47 of the

active pocket and the pyrrole-N of NRCB. The binding free energy of hydrogen bond interactions is -8.43 kcal/mol. The docking analyses indicate that these amino acid residues are in the regions of the two average structures of P-selectin,²⁸ and therefore NRCB would be a potential inhibitor. This encouraged the present paper synthesized NRCB, imaged the nano-feature, and evaluated the *in vitro/in vivo* activities.

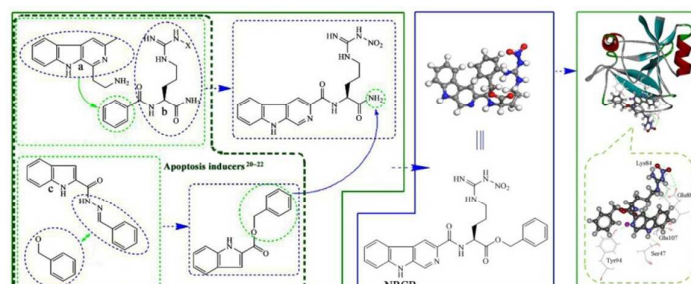
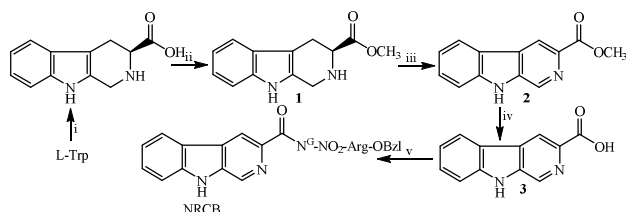


Fig. 1 The analyses of the pharmacophores of three apoptosis inducers, the rational replacement of $\text{NH}-\text{N}=\text{CH}-\text{C}_6\text{H}_5$ with $\text{OCH}_2\text{C}_6\text{H}_5$, the conformational optimization and the docking towards the active site of P-selectin lead to the design of NRCB as a novel apoptosis inducer.

Results and discussion

Synthesis of NRCB

Based on **Scheme 1** NRCB was prepared via five-step reactions. The yields of five step reactions were 98%, 43%, 47%, 88% and 27%, respectively. The related data are provided in the ESI.† The appropriate conditions and the simple procedure showed that the synthetic route was suitable for preparing NRCB.



Scheme 1 Synthetic route of NRCB. i) CH_2O , H_2O and concentrated sulfuric acid; ii) CH_3OH and SOCl_2 ; iii) Acetone and KMnO_4 ; iv) Methanol aqueous NaOH (4 M); v) L-Arg(NO_2)-OBzl, N-methylmorpholine, 1-(3-dimethylaminopropyl)-3-ethylcarbodiimide (EDC), N-hydroxybenzotriazol (HOBt) and N,N-dimethylformamide (DMF).

Apoptosis activity of NRCB *in vitro*

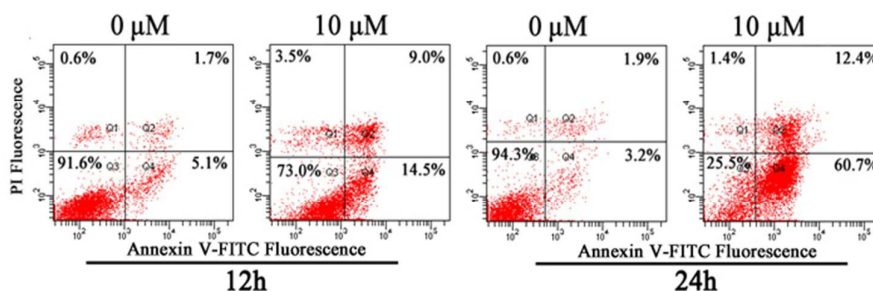


Fig. 2 Time-dependent change of Annexin V-FITC and PI intensity of K562 cells treated with $10 \mu\text{M}$ of NRCB, Q4 (Annexin V+ and PI-) represents for early apoptotic cells, Q2 (Annexin V+ and PI+) represents for late apoptotic cells.

Fig. 3D - Fig. 3F are the SEM images of the solids resulted from 0.1, 1.0 and $10.0 \mu\text{M}$ aqueous solutions of NRCB. **Fig. 3D** indicates that the form of the solids resulted from $0.1 \mu\text{M}$ aqueous solution of NRCB is nanoparticles of 28.6 - 88.9 nm in

The rationality of the design of NRCB as apoptosis inducer was confirmed by flow cytometry assay, and the suspension K562 cells were used for this assay in particular. **Fig. 2** indicates that the total apoptosis percentages of K562 cells treated with $10 \mu\text{M}$ of NRCB for 12 h and 24 h are 23.5% and 73.1%, respectively, showing a time-dependent increase and ensuring NRCB been an apoptosis inducer.

Nano-feature and benefits of NRCB

The nano-feature of NRCB in aqueous solution, in solid state and in rat plasma was visualized with TEM, SEM and AFM images. The nano-property of aqueous solution of NRCB was characterized with Faraday-Tyndall effect, size and zeta potential. To estimate the molecular number in an individual nanoparticle mesoscale simulation was performed.

Fig. 3A - Fig. 3C are the TEM images of 0.1, 1.0 and $10.0 \mu\text{M}$ of NRCB aqueous solutions. **Fig. 3A** indicates that in $0.1 \mu\text{M}$ aqueous solution NRCB forms nanoparticles of 8.0-72.7 nm in diameter. **Fig. 3B** indicates that in $1.0 \mu\text{M}$ aqueous solution NRCB forms nanoparticles of 10.8-116.1 nm in diameter. **Fig. 3C** indicates that in $10.0 \mu\text{M}$ aqueous solution NRCB forms nanoparticles of 43.9-176.3 nm in diameter. Thus the nanoparticle size of NRCB in ultrapure water depends on the concentration.

diameter. **Fig. 3E** indicates that the form of the solids resulted from $1.0 \mu\text{M}$ of aqueous solution of NRCB is nanoparticles of 33.3-100.0 nm in diameter. **Fig. 3F** indicates that the form of the solids resulted from $10.0 \mu\text{M}$ of aqueous solution of NRCB is

nanoparticles of 44.4-111.1 nm in diameter. Thus the nanoparticle size of the solids depends on the concentration of the aqueous solution of NRCB.

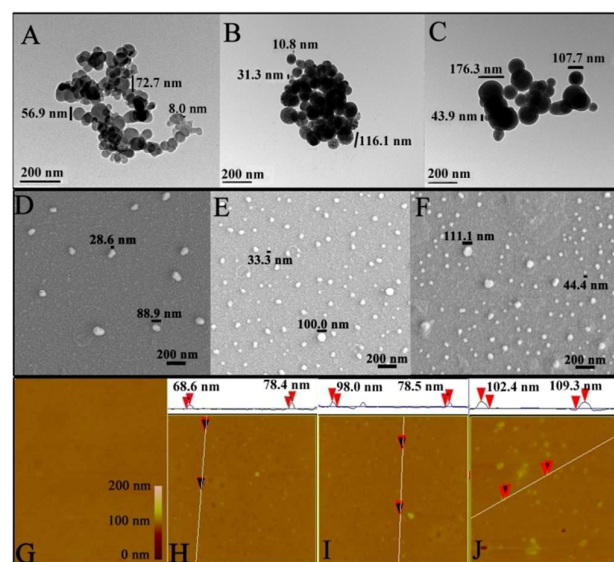


Fig. 3 TEM, SEM and AFM images of NRCB. (A) TEM image of 0.1 μM solution of NRCB in ultrapure water; (B) TEM image of 1.0 μM solution of NRCB in ultrapure water; (C) TEM image of 10.0 μM solution of NRCB in ultrapure water; (D) SEM image of the solids formed by 0.1 μM aqueous solution of NRCB; (E) SEM image of the solids formed by 1.0 μM aqueous solution of NRCB; (F) SEM image of the solids formed by 10.0 μM aqueous solution of NRCB; (G) AFM image of rat plasma alone; (H) AFM image of 0.1 μM solution of NRCB in rat plasma; (I) AFM image of 1.0 μM solution of NRCB in rat plasma; (J) AFM image of 10.0 μM solution of NRCB in rat plasma.

Fig. 3G - Fig. 3J are the AFM images of 0.1, 1.0 and 10.0 μM solutions of NRCB in rat plasma. **Fig. 3H** indicates that in rat plasma and at 0.1 μM concentration NRCB forms nanoparticles of 68.6-78.4 nm in high. **Fig. 3I** indicates that in rat plasma and at 1.0 μM concentration NRCB forms nanoparticles of 78.5-98.0 nm in high. **Fig. 3J** indicates that in rat plasma and at 10.0 μM concentration NRCB forms nanoparticles of 102.4-109.3 nm in high. Thus the nanoparticle size of NRCB in rat plasma depends on the concentration. In rat plasma NRCB formed nanoparticles of >110 nm in high suggests that NRCB's nanoparticles would not be phagocytized by macrophages and can safely deliver in blood circulation.²⁹

The nano-property of NRCB's aqueous solution is characterized with Faraday-Tyndall effect, size and zeta potential. **Fig. 4A** and **4B** indicate that ultrapure water and the solution of NRCB in ultrapure water (1 μM) are clean. **Fig. 4C** indicates that in the irradiation of 650 nm laser beam ultrapure water occurs no Faraday-Tyndall effect, while the irradiation of 650 nm laser beam induces the solution of NRCB in ultrapure water (1 μM) to occur Faraday-Tyndall effect (**Fig. 4D**). Thus Faraday-Tyndall effect evidences 1 μM solution of NRCB in ultrapure water having nano-property. The solution is further explained with mean size (~165 nm), which ensures the solution having nano-property and the particles having stable size. **Fig. 4F** shows that 1 μM solution of NRCB in ultrapure possesses -14.2 mV of zeta potential, and the half width of the peak is 5.86 mV. Thus Faraday-Tyndall effect,

size and zeta potential consistently support that in ultrapure water NRCB forms nano-solution.

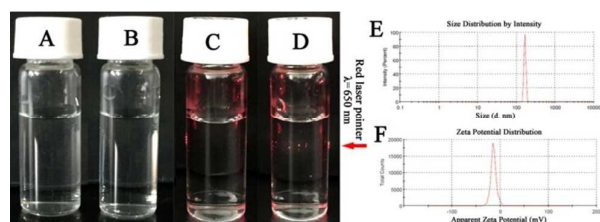


Fig. 4 Characterizing the nano-property of NRCB's aqueous solution. (A) Ultrapure water without radiation; (B) NRCB in ultrapure water (1 μM) without radiation; (C) Ultrapure water with 650 nm laser radiation; (D) NRCB in ultrapure water (1 μM) with 650 nm laser radiation; (E) Size of NRCB in ultrapure water (1 μM); (F) Zeta potential of NRCB in ultrapure water (1 μM).

Mesoscale simulation was used to predict the molecular number of NRCB in a nanoparticle of fixed size. **Fig. 5** indicates that three "beads" are constructed by atomistic simulations and placed at the center-of-mass groups of atoms on the particular parts of the molecule of NRCB. The calculation assisted by mesoscale simulation software shows that, employing the monomer as a building block, 1428 of molecules can form a nanoparticle of 10.4 nm in diameter. Accordingly, in the smallest nanoparticles of 8.0 nm, 10.8 nm and 43.9 nm in diameter of **Fig. 3A**, **Fig. 3B** and **Fig. 3C** contain 1098, 1483 and 6028 of molecules of NRCB, respectively.

FT-MS and NOESY 2D NMR spectra defined NRCB forming hexamers

The FT-MS spectrum of NRCB in water are shown in **Fig. 6A** which gives a positive ion peak at 1510.58526 of the mass of a hexamer plus H, a positive ion peak at 1258.99049 of the mass of a pentamer plus H, a positive ion peak at 2013.79361 of the mass of a tetramer plus H, a positive ion peak at 1510.58526 of the mass of a trimer plus H, a positive ion peak at 1007.39241 of the mass of a dimer plus H, and a positive ion peak at 504.19815 of the mass of a monomer plus H. The qCID spectra (**Fig.S4** in Supporting Information) indicate that the pentamer, tetramer, trimer, dimer and monomer are the fragmentation products of the hexamer. Therefore the hexamer is the sole form of NRCB existed in water.

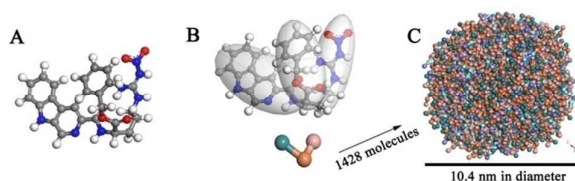


Fig. 5 Mesoscale simulation software assisted calculation. A nanoparticle of 10.4 nm in diameter contains 1428 of NRCB molecules.

To show the interaction pattern the molecule in a hexamer the NOESY 2D NMR spectrum of NRCB was recorded with the standard method. **Fig. 6B** gives three interesting cross-peaks. Cross-peak 1 is resulted from the interaction of $\text{CH}_2\text{-CH}_2\text{-CH}_2\text{-NH-C=NH(NH-NO}_2\text{)}$ of one molecule with the H of carboline-3-CONH of another molecule. Cross-peak 2 is resulted from the interaction of $\text{CH}_2\text{-CH}_2\text{-CH}_2\text{-NH-C=NH(NH-NO}_2\text{)}$ of one molecule with the H on the 2-position of the benzyl of another molecule, as well as the interaction of $\text{CH}_2\text{-CH}_2\text{-CH}_2\text{-NH-}$

C=NH(NH-NO₂) of one molecule with the aromatic H at 7-position of the carboline residue of another molecule. Cross-peak3 is resulted from NH-C=NH(NH-NO₂) of one molecule with the aromatic H at 7-position of the carboline residue of another molecule. These distances between the mentioned hydrogen atoms are less than 4 Å, which reflects an approaching manner of six

molecules with minimal energy conformation. Accordingly, the hexamer has triangle like conformation (**Fig. 6C**).

Using FT-MS and NOESY 2D NMR spectra to define the hexamer of NRCB and to establish the triangle like conformation of the hexamer are of interest not only for exploring the intermolecular association of small molecule but also for analyzing the chemical mechanism of small molecule to form nanoparticle.

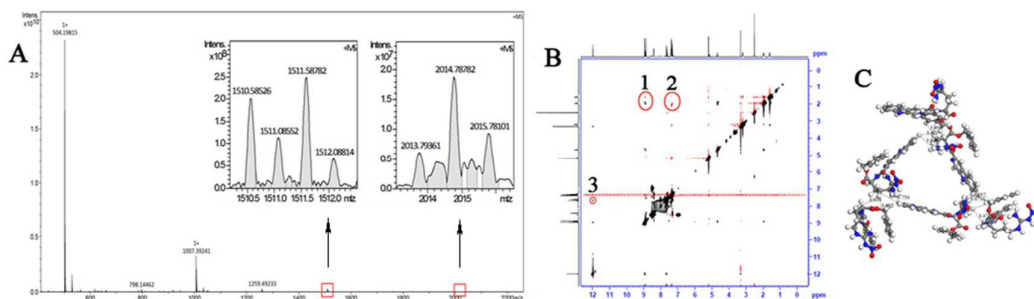


Fig. 6 FT-MS spectrum, NOESY 2D NMR spectrum and 3D structure of the hexamer. (A) FT-MS spectrum of NRCB, in which the ion peaks of the hexamer, pentamer, tetramer and trimer are amplified; (B) NOESY 2D NMR spectrum of NRCB, in which three interesting cross-peaks are labeled with red rings; (C) Triangle like conformation of the hexamer formed by six molecules in the minimal energy conformation, the approaching manner of six molecules been defined by the NOESY 2D NMR spectrum.

In vitro activities of NRCB

The *in vitro* activities of NRCB were evaluated with anti-proliferation assay and CT-DNA intercalation assay. Anti-proliferation assay explored the *in vitro* activities of NRCB inhibiting the proliferation of HCT-8, HL60, A549, SH-sy5y, HeLa, HT-29 and K562 cells, which are represented with IC₅₀ values and shown in **Fig. 7A**. According to the IC₅₀ values of NRCB against the proliferation of seven cell lines, K562 cells are the most sensitive cells, while HeLa cells are the most insensitive cells. Since the IC₅₀ values range from 15.3 μM to 74.1 μM, therefore NRCB can moderately inhibit the proliferation of seven cell lines *in vitro*.

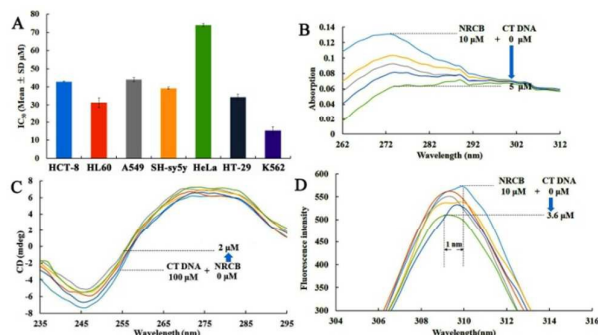


Fig. 7 *In vitro* activities of NRCB. (A) Effects of NRCB on cancer cell proliferation (n=3); (B) UV spectrum of 10 μM of NRCB with increased amount of CT DNA; (C) CD spectra of 100 μM of CT DNA with increased amount of NRCB; (D) Fluorescence spectra of 10 μM of NRCB with increased amount of CT DNA.

Since the apoptosis inducer can intercalate into CT-DNA,^{30,31} the intercalation activity of NRCB against CT DNA is visualized with the changes of UV, circular dichroism (CD) and fluorescence spectra of NRCB or CT DNA.

Fig. 7B indicates that with the concentration of CT DNA been from 0 μM increased to 5 μM the UV absorption intensity of NRCB

been concentration dependently decreased. **Fig. 7C** indicates that with the concentration of NRCB been from 0 μM increased to 2 μM the molecular ellipticities [θ] of positive and negative bands of CT DNA been concentration dependently increased. **Fig. 7D** shows the typical course of the fluorescence quenching, the fluorescence intensity of NRCB gradually decreased with the concentration of CT DNA been from 0 μM gradually increased to 3.6 μM. When the concentration of the CT DNA increased to 3.6 μM, the fluorescence intensity of NRCB lowered to its minimum. Over the course of the fluorescence quenching 1 nm of bathochromic shift is also noticed. This bathochromic shift is considered to be associated with a decrease in the energy gap between the highest and lowest occupied molecular orbital, and results from intercalation of NRCB with CT DNA.

All the spectra based observations reflect the intercalation of NRCB with CT DNA and are characterized by decreasing both the base stacking and the right-handedness of CT DNA, therefore evidence NRCB is an apoptosis inducer.

Confocal images of NRCB treated cancer cells

To understand the *in vitro* anti-proliferation and intercalation activities of NRCB for the cancer cells the confocal images of 40 μM of NRCB treated HeLa, SH-sy5y and HT-29 cells were selected as the representatives to visualize the distribution of NRCB inside the cells. **Fig. 8A** indicates that after 12 h-treatments the amounts of NRCB inside the nuclei of HeLa, SH-sy5y and HT-29 cells are HeLa<SH-sy5y<HT-29. This is in accordance of the IC₅₀ values of NRCB against HeLa, SH-sy5y and HT-29 cells are HeLa>SH-sy5y>HT-29. **Fig. 8A** also indicates that after 24 h-treatments the amount of NRCB inside the nuclei of HeLa, SH-sy5y and HT-29 cells increases, suggesting the amount of NRCB entering the nuclei of the cancer cells depended on the treated time.

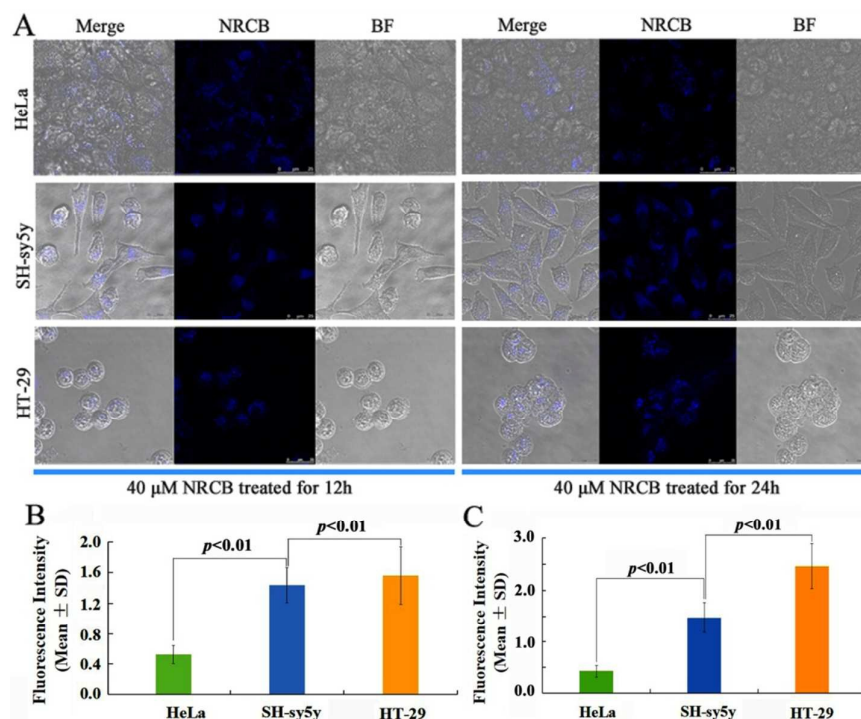


Fig. 8 Confocal images and fluorescent intensity of 40 μM of NRCB treated cancer cells. (A) Confocal images of HeLa, SH-sy5y and HT-29 cells treated with 40 μM NRCB for 12 and 24 h; (B) Fluorescence intensities inside the nuclei of HeLa, SH-sy5y and HT-29 treated with 40 μM NRCB for 12h; (C) Fluorescence intensities inside the nuclei of HeLa, SH-sy5y and HT-29 treated with 40 μM NRCB for 24h.

***In vivo* activities of NRCB**

The utility of NRCB as a novel apoptosis inducer was finally evidenced by it slowing the tumor growth of S180 mice, down-regulating P-selectin expression, decreasing the serum concentration of TNF- α , depressing xylene induced ear edema of the mice and reducing the serum concentration of IL-2.

Fig. 9A shows the tumor weights of S180 mice treated with CMCNa, 2 $\mu\text{mol/kg}$ of doxorubicin (Dox) and NRCB at 0.01, 0.1 and 1 $\mu\text{mol/kg}$ of doses. As seen, the tumor weight of S180 mice treated with CMCNa is significantly higher than that of S180 mice treated with 0.01 $\mu\text{mol/kg}$ of NRCB, suggesting the minimal effective dose of NRCB in slowing tumor growth is 0.01 $\mu\text{mol/kg}$. The tumor weights of S180 mice treated with NRCB decrease significantly with the dose been increased from 0.01 $\mu\text{mol/kg}$ to 0.1 $\mu\text{mol/kg}$ and 1 $\mu\text{mol/kg}$, suggesting a dose dependent action. The tumor weights of S180 mice treated with 2 $\mu\text{mol/kg}$ of Dox equal to that of S180 mice treated with 1 $\mu\text{mol/kg}$ of NRCB, suggesting the *in vivo* anti-tumor activity of NRCB been 2 folds higher than

that of Dox. If the anti-tumor activity is represented with tumor size the similar activity relationships are also clear (see **Fig. 9B**).

Fig. 9C shows that NRCB dose dependently decreases the serum concentration of P-selectin of the treated S180 mice. Due to tumor growth can be significantly slowed in the absence of P-selectin and high tumor cell apoptosis can be observed in the tumor growing in P-selectin $-/-$ mice,²⁷ the serum concentration of P-selectin of S180 mice been dose dependently decreased by NRCB evidences that NRCB is an apoptosis inducer capable of decreasing serum concentration of P-selectin.

Fig. 9D shows that NRCB dose dependently decreases the serum concentration of TNF- α of the treated S180 mice. Though relevant rise of TNF- α was found in fracture patients *in vivo* and the enhancement of apoptosis was found in TNF- α treated osteoblast cells *in vitro*,³² the finding that NRCB simultaneously slows tumor growth and decreases serum concentration of TNF- α of S180 mice in a dose dependent manner demonstrates that the causality of TNF- α and apoptosis is an inherent correlation.

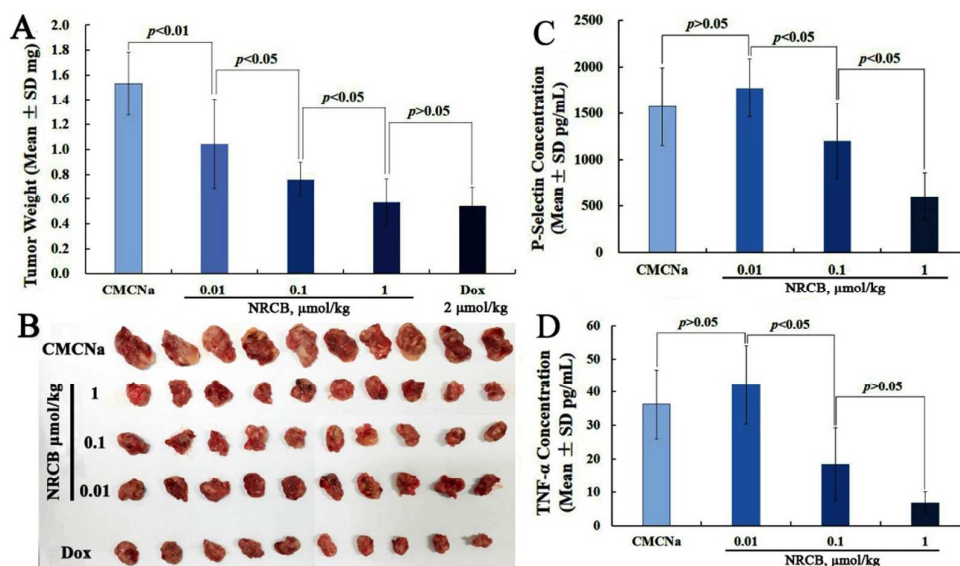


Fig. 9 *In vivo* anti-tumor P-selectin down-regulation and TNF- α inhibition activities of NRCB. (A) Tumor weights of S180 mice treated with NRCB at three doses, $n=10$; (B) Tumor sizes of S180 mice treated with NRCB at three doses, $n=10$; (C) Serum P-selectin of S180 mice treated with NRCB at three doses, $n=5$; (D) Serum TNF- α of S180 mice treated with NRCB at three doses, $n=5$.

Simultaneously reducing ear edema and the concentration of serum TNF- α and IL-2 of xylene treated mice are another profile of *in vivo* activities of NRCB. **Fig. 10A** indicates that the ear edema of the mice treated with 1 $\mu\text{mol/kg}$ of NRCB is significantly lower than that of the mice treated with NS and 16.7 $\mu\text{mol/kg}$ of aspirin, suggesting 1 $\mu\text{mol/kg}$ of NRCB been able to inhibit xylene induced inflammatory response and its potency been 16.7 folds higher than that of aspirin. **Fig. 10B** indicates that the concentrations of serum TNF- α and IL-2 of edema mice treated with 1 $\mu\text{mol/kg}$ of NRCB are significantly lower than that of the mice treated with NS, suggesting 1 $\mu\text{mol/kg}$ of NRCB been able to effectively decrease the concentrations of serum TNF- α and IL-2 of inflammatory mice. Due to IL-2 is a physiologic inhibitor of apoptosis,³³ the decrease of serum TNF- α and IL-2 concentrations of inflammatory mice could be a result of 1 $\mu\text{mol/kg}$ of NRCB inhibits TNF- α and IL-2 production, thereby promotes apoptosis.

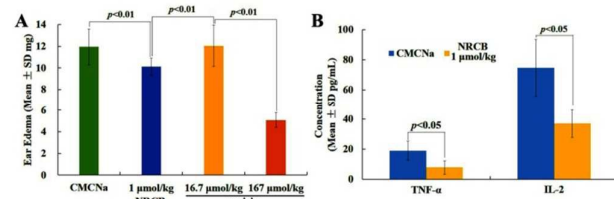


Fig. 10 Xylene induced ear edema, serum TNF- α and serum IL-2 of the mice treated with NRCB. (A) Xylene induced ear edema of the mice treated with 1 $\mu\text{mol/kg}$ of NRCB; (B) Serum TNF- α and IL-2 of ear edema mice treated with 1 $\mu\text{mol/kg}$ of NRCB.

Experimental

The detailed methodologies and data for all experiments are given as ESI,[†] and simply described in Reference 34 as the notes. Sprague Dawley rats and ICR mice were purchased from the Animal Center of Peking University. Work performed was based on a protocol reviewed and approved by the ethics committee of Capital Medical University. The committee assures that the welfare of the animals was maintained in accordance with the requirements of the Animal Welfare Act.

Conclusions

The analysis of three apoptosis inducer as shown in Figure 1,²⁰⁻²² the docking towards the active site of P-selectin and the mesoscale simulation can lead to discovering NRCB as a nanoscale apoptosis inducer capable of decreasing serum concentrations of P-selectin, TNF- α and IL-2 of the mice. *In vitro* NRCB is able to promote the apoptosis of cancer cells, to intercalate into the DNA of the cancer cells, to enter the nuclei of the cancer cells, to inhibit the proliferation of cancer cells and to form nanoparticles of suitable size for delivering in blood circulation. *In vivo* 0.01, 0.1 and 1 $\mu\text{mol/kg}$ of NRCB slow tumor growth, decrease serum concentrations of P-selectin and TNF- α in a dose-dependent manner. At 1 $\mu\text{mol/kg}$ of dose NRCB also effectively inhibits ear edema and reduces the serum levels of TNF- α and IL-2 of xylene

treated mice. NRCB is a promising lead compound of apoptosis inducer for chemotherapy.

Acknowledgements

This work was supported by Beijing Municipal Science & Technology Commission (Z141100002114049), the NSFC (81273379, 81270046, 81373264 and 81373265), Beijing Natural Science Foundation (7162025), KZ201610025029, TJSHG201310025008, and 863 program (2015AA020902).

References

- 1 G. Kroemer, W. El-Deiry, P. Golstein, M. Peter, D. Vaux, P. Vandenabeele, B. Zhivotovsky, M. Blagosklonny, W. Malorni and R. Knight, *Cell Death Differ.*, 2005, **12**, 1463-1467.
- 2 M. Nazari, A. Minai-Tehrani and R. Emamzadeh, *RSC Adv.*, 2014, **4**, 45128-45135.
- 3 F. Radogna, M. Dicato and M. Diederich, *Biochem. Pharmacol.*, 2015, **94**, 1-11.
- 4 Y. Kondo, T. Kanzawa, R. Sawaya and S. Kondo, *Nat. Rev. Cancer*, 2005, **5**, 726-734.
- 5 H. Kawasaki, M. Toyoda, H. Shinohara, J. Okuda, I. Watanabe, T. Yamamoto, K. Tanaka, T. Tenjo and N. Tanigawa, *Cancer*, 2001, **91**, 2026-2032.
- 6 J.C. Reed, *Nat. Rev. Drug Disc.*, 2002, **1**, 111-121.
- 7 S.W. Fesik, *Nat. Rev. Cancer*, 2005, **5**, 876-885.
- 8 C.B. Thompson, *Science*, 1995, **267**, 1456-1462.
- 9 J.C. Reed and K.J. Tomaselli, *Curr Opin Biotechnol*, 2000, **11**, 586-592;
- 10 M. Tolomeo and D. Simoni, *Curr. Med. Chem. AntiCancer Agents*, 2002, **2**, 387-401.
- 11 H. Wang, S.L. Yeo, J. Xu, X. Xu, H. He, F. Ronca, A.E. Ting, Y. Wang, V.C. Yu and M.M. Sim, *J. Nat. Prod.*, 2002, **65**, 721-724.
- 12 C.M. Jakobsen, S.R. Denmeade, J.T. Isaacs, A. Gady, C.E. Olsen and S.B. Christensen, *J. Med. Chem.*, 2001, **44**, 4696-4703.
- 13 D. Simoni, M. Roberti, F.P. Invidiata, R. Rondanin, R. Baruchello, C. Malagutti, A. Mazzali, M. Rossi, S. Grimaudo, F. Capone, L. Dusonchet, M. Meli, M.V. Raimondi, M. Landino, N. D'Alessandro, M. Tolomeo, D. Arindam, S. Lu and D.M. Benbrook, *J. Med. Chem.*, 2001, **44**, 2308-2318.
- 14 R.F. George, M.A. Fouad and I.E.O. Goma, *Eur. J. Med. Chem.*, 2016, **112**, 48-59.
- 15 X. Huang, R. Huang, Z. Liao, Y. Pan, S. Gou, H. Wang, *Eur. J. Med. Chem.*, 2016, **108**, 381-391.
- 16 S. Yang, M. Liu, H. Xiang, Q. Zhao, W. Xue and S. Yang, *Eur. J. Med. Chem.*, 2015, **102**, 249-255.
- 17 H. Zhang, Y. Liu, T. Meng, Q. Qin, S. Tang, Z. Chen, B. Zou, Y. Liua and H. Liang, *Med. Chem. Commun.*, 2015, **6**, 2224-2231.
- 18 A. Daoud, J. Song and F. Xiao, *Eur. J. Pharmacol.*, 2014, **724**, 219-230.
- 19 H. Zhang, K. Sun and J. Ding, *Phytomedicine*, 2014, **21**, 348-355.
- 20 T.A. Mansoor, R.M. Ramalho, S. Mulhovo, C.M.P. Rodrigues and M.J. Ferreira, *Bioorg. Med. Chem. Letters*, 2009, **19**, 4255-4258.

- 21 H. Zhang, J. Drewe, B. Tseng, S. Kasibhatla and S.X. Cai, *Bioorg. Med. Chem.*, 2004, **12**, 3649-3655.
- 22 J. Slack, C. Causey and P. Thompson, *Cell. Mol. Life Sci.*, 2011, **68**, 709-720.
- 23 S. Huerta and G. Baay, *Nitric Oxide*, 2009, **20**, 182-94.
- 24 M. Matsumoto, W. Nakajima, M. Seike, A. Gemma and N. Tanaka, *Biochemical and Biophysical Research Communications*, 2016, **473**, 490-496.
- 25 H. Mizutani, S. Tada-Oikawa, Y. Hiraku, M. Kojima and S. Kawanishi, *Life Sciences*, 2005, **76**, 1439-1453.
- 26 S. Gao, H. Li, H. Feng, M. Li, Z. Liu, Y. Cai, J. Lu, X. Huang, J. Wang, Q. Li, S. Chen, J. Ye and P. Liu, *Journal of Molecular & Cellular Cardiology*, 2014, **79C**, 92-103.
- 27 T.H. Nasti, D.C. Bullard and N. Yusuf, *Life Sci.*, 2015, **131**, 11-18.
- 28 H. Zhu, Y. Wang, M. Zhao, J. Wu, X. Zhang, G. Yang and S. Peng, *MedChemComm*, 2013, **4**, 1066 - 1072.
- 29 Y. Fujita, M. Mie and E. Kobatake, *Biomaterials*, 2009, **30**, 3450-3457.
- 30 P. Mondal, S. Roy, G. Loganathan, B. Mandal, D. Dharumadurai, M.A. Akbarsha, P.S. Sengupta, S. Chattopadhyay and P.S. Guin, *Biochemistry and Biophysics Reports*, 2015, **4**, 312-323.
- 31 B. Demoulin, M. Hermant, C. Castrogiovanni, C. Staudt and P. Dumont, *Toxicol. In Vitro*, 2015, **29**, 1156-1165.
- 32 M. Sun, J. Yang, J. Wang, T. Hao, D. Jiang, G. Bao, G. Liu, *Cytokine*, 2016, **80**, 35-42.
- 33 T.A. Fleisher, *Ann. Allergy Asthma Immunol.*, 1997, **78**, 245-250.
- 34 Notes: 1) **Flow cytometry assay**: to explore the apoptosis activity of NRCB, flow cytometry assay was recorded. K562 cells (10^6 cells/mL) were incubated in 1640 Medium at 37°C in a humidified atmosphere containing 5% CO₂ for 4 h. A solution of NRCB (final concentration: 10 μM, in complete 1640 medium as above; 2.5 mL/well) was added, and cells were incubated at 37°C in a humidified atmosphere (containing 5% CO₂) for 12 h and 24 h. After removing the medium, the cells were washed by fresh medium (1 mL×2) and stained with Annexin V-FITC (KeyGEN Biological Technology Co., Ltd., Nanjing, PR China) and Propidium Iodide (PI) for 10 minutes. PI and FITC fluorescence for cells was analyzed for ~10,000 events (counts) per sample aliquot. 2) **TEM test**: Shape and size examinations of the NRCB nanospecies were performed with transmission electron microscopy (TEM, JSM-6360 LV, JEOL, Tokyo, Japan). An aqueous solution of NRCB (pH 7.0) was dripped onto a formvar-coated copper grid, and then a drop of anhydrous ethanol was added to promote water removal. Then the grid was first allowed to dry thoroughly in air and it was then heated at 37°C for 24 h. The samples were viewed under TEM. The shape and size distributions of the nanospecies were determined by counting >100 species in randomly selected regions on the TEM copper grid. All of the determinations were carried out on triplicate grids. The TEM was operated at 80 kV (the electron beam accelerating voltage). Images were recorded on an imaging plate (Gatan Bioscan Camera Model 1792; Gatan, Inc., Pleasanton, CA, USA) with 20 eV energy windows at 6,000-400,000× and they were digitally enlarged. 3) **SEM test**: the shape and size of the nanospecies in lyophilized powders were measured

ARTICLE

Journal Name

by scanning electron microscopy (SEM, JEM-1230; JEOL) at 50 kV. The lyophilized powders were attached to a copper plate with double-sided tape (Euromedex, Souffelweyersheim, France). The specimens were coated with 20 nm gold-palladium using a JEOL JFC-1600 Auto Fine Coater. The coater was operated at 15 kV, 30 mA, and 200 mTorr (argon) for 60 seconds. The shape and size distributions of the nanoparticles were measured by examining > 100 particles in randomly selected regions on the SEM alloy. All measurements were performed on triplicate grids. Images were recorded on an imaging plate (Gatan Bioscan Camera Model 1792; Gatan, Inc.) with 20 eV energy windows at 100–10,000 \times , and they were digitally enlarged. **4) AFM test:** Atomic force microscopy (AFM) images were obtained using the contact mode on a Nanoscope 3D AFM (Veeco Instruments, Inc., Plainview, NY, USA) under ambient conditions. Samples of NRCB in rat plasma (10^{-6} M) were used for recording the images. **5) Faraday-Tyndall effect of NRCB:** 1 μ M solution of NRCB in ultrapure water was irradiated with laser beam of 650 nm. In addition, the zeta potential and size were determined on a Malvern's Zetasizer (Nano-ZS90; Malvern Instruments) with the DTS Program.

Graphical Abstract

